Supporting Information

accompanying "A simple stomatal model that unifies the metabolic and hydraulic control of carbon and water flux" by TN Buckley et al (Global Change Biology, 2026)

Contents:

Table S1. Model performance statistics for Dataset #1. Bolded values represent the highest performance for given species and parameter sets. In column 1, "different" means that each model was fitted separately for the control treatment and the drought treatment, so that there were two sets of parameters for each species; "same" means that each model was fitted to both treatments combined, so that there was only a single set of parameters for each species.

parameters for control and drought treatment	species		RMSE (Eqn 3)	RMSE (USO)	RMSE (BB)		r^2_{adj} (Eqn 3)	r^2_{adj} (USO)	r^2_{adj} (BB)
different	grapevine		**0.0102**	0.0136	0.0142		**0.980**	0.969	0.966
	olive		0.0130	0.0122	**0.0118**		0.859	0.881	**0.889**
	almond		0.0283	**0.0272**	0.0488		0.750	**0.783**	0.468
same	grapevine		**0.0101**	0.0796	0.0716		**0.981**	0.186	0.131
	olive		**0.0209**	0.0348	0.0339		**0.623**	0.033	0.144
	almond		**0.0302**	0.0522	0.0695		**0.710**	0.193	-0.064

Table S2. Mean parameters fitted for the new model (in the form given by Eqn 5) and the USO model for Dataset #2. *n*: number of species × site combinations fitted in each group. r^2_{adj}: median adjusted correlation coefficient between observed and predicted g_{sw} across species × site combinations E_m, p, g_1: medians ± median absolute deviations. Units: E_m (mmol m^{-2} s^{-1}), p (nmol m^{-2} s^{-1}), g_1 ($kPa^{0.5}$).

group	*n*	E_m	*p*	r^2_{adj} (Eqn 5)	g_1	r^2_{adj} (USO)
by aridity zone						
arid	9	17.4 ± 21.4	240.3 ± 258.2	0.38	3.5 ± 1.18	0.65
dry sub-humid	15	1.9 ± 1.6	8.4 ± 12.4	0.06	3.3 ± 1.85	0.41
humid	102	6.2 ± 5.3	73.5 ± 95.6	0.46	3.9 ± 1.84	0.65
semi-arid	14	5.2 ± 5.4	41.7 ± 34.6	0.53	2.9 ± 1.08	0.76
by biome						
arctic	8	1.0 ± 0.4	0.0001 ± 0	-0.01	2.2 ± 1.59	0.24
boreal	5	3.8 ± 3.6	49.9 ± 64.4	0.46	1.7 ± 0.61	0.69
temperate	76	6.2 ± 5.6	78.4 ± 88.7	0.46	4.1 ± 1.94	0.69
tropical	51	6.2 ± 6.1	91.9 ± 136.3	0.41	3.5 ± 1.22	0.64
by major evolutionary group						
angiosperm	126	6.2 ± 6.2	82.1 ± 109.8	0.4	3.8 ± 1.62	0.64
gymnosperm	14	2.2 ± 1.3	21.9 ± 18.2	0.53	2.1 ± 0.63	0.69
by functional type						
crop	5	20.3 ± 22.9	182.3 ± 240.6	0.36	5.8 ± 1.85	0.72
grass	17	15.8 ± 7.5	218 ± 216.5	0.29	4.6 ± 1.14	0.52
savanna	20	11.7 ± 8.9	195.9 ± 290.5	0.45	3.5 ± 1.1	0.72
shrub	16	2.2 ± 2	16.8 ± 24.9	0.3	3.3 ± 1.8	0.46
tree	82	4 ± 3.1	50.2 ± 61	0.47	3.3 ± 1.46	0.7

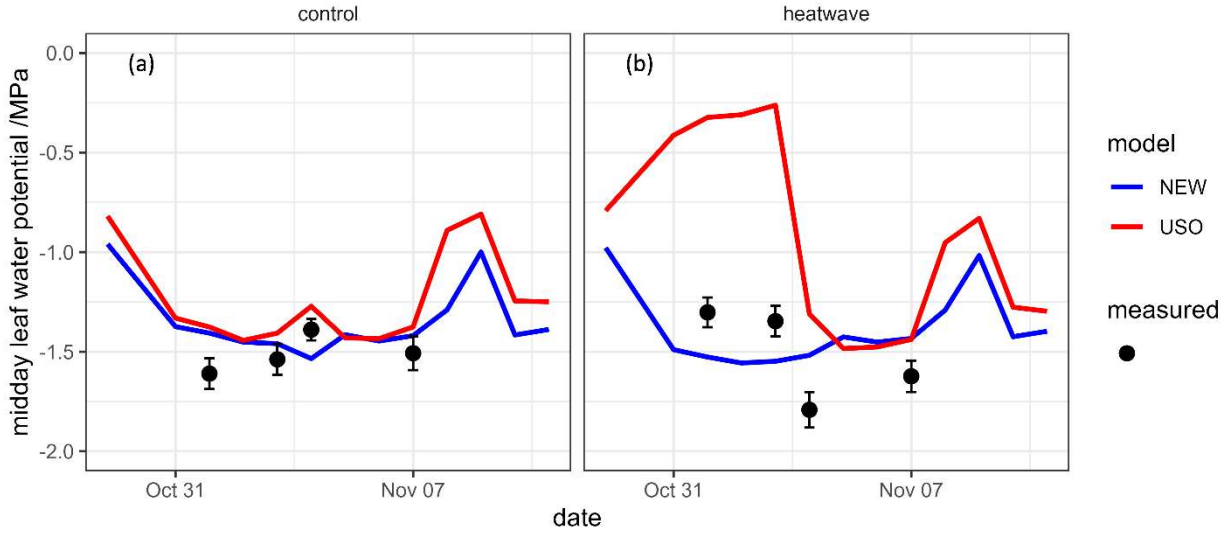

Figure S1. Trends in midday leaf water potential under control conditions (a; daily max temperature 28-29°C) or during a four-day heatwave (b; daily max air temperature 43-44°C), measured for *Eucalyptus parramattensis* trees (black symbols; error bars are ± SE) or simulated by the new model (blue lines) or the USO model (red lines). Soil water had been withheld from both control and heatwave trees for 30 days prior to the experiment. Original data from Drake et al. (2018), with USO simulations from Sicangco et al. (2026) (cf. their Figure 5). The heatwave was imposed from 31 October to 03 November (2016), corresponding to the first three water potential measurements shown here.

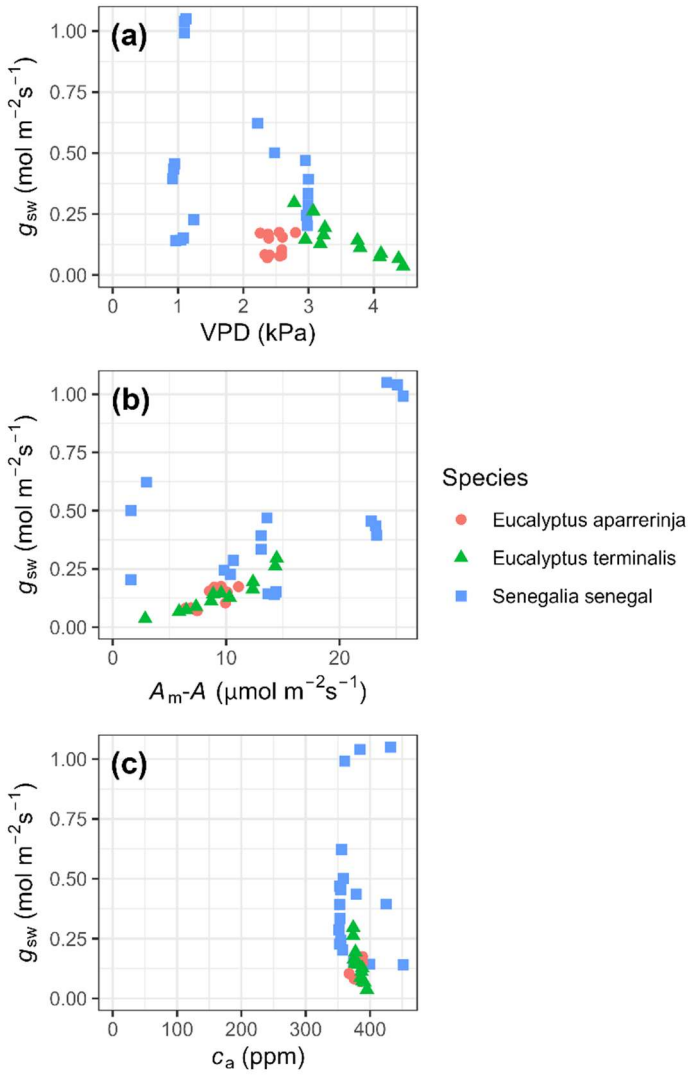

Figure S2. Relationships of g_{sw} with VPD (a), residual photosynthetic capacity ($A_m - A$, (b)), and ambient CO_2 (c_a, (c)), for the three arid-environment species for which fitted values of E_m and p were several orders of magnitude larger than for other arid species. For *S. senegal*, g_{sw} was unrelated to VPD, and not because of countervailing influences of $A_m - A$ or c_a (b,c). For *E. aparrerinja*, VPD varied minimally in the dataset. For *E. terminalis*, $A_m - A$ increased strongly as VPD increased, and not because stomatal closure reduced assimilation rate (c_i, not shown, was nearly constant); this nullified the effect of Δw in the denominator of Eqn 5, making stomata appear insensitive to VPD. Each of these patterns would cause the fitting algorithm to identify very large values for both E_m and p, equivalent to low VPD sensitivity.

Figure S3. Figure 5 from the main text is reproduced here, in two forms: first (left) including all points (identical to Fig 5), and second (right), excluding the 13 points for which nls() in R could not successfully fit parameters for Eqn 5, so estimates from a linear fit to an inverted form of the model were used instead, as described in Methods S3. None of the patterns are discernibly affected by exclusion or inclusion of those 13 points. *This is the legend from Fig 5: Distributions of parameter values for the new model (in the form given by Eqn 5, with parameters E_m and p) and the USO model (with parameter g_1) fitted to data of Lin et al.* (2015)*, within various subgroupings as given by Lin et al.: (a-c): plant functional types ('savanna' refers to 'savanna trees' as defined by Lin et al.); (d-f): latitudinal zones (as defined by Lin et al.); (g-i): gymnosperms vs. angiosperms; (j-l): regions of differing aridity. Medians are shown with vertical lines, and are also listed in Table S2, along with numbers of species × site combinations in each category and corresponding median adjusted r^2 values.*

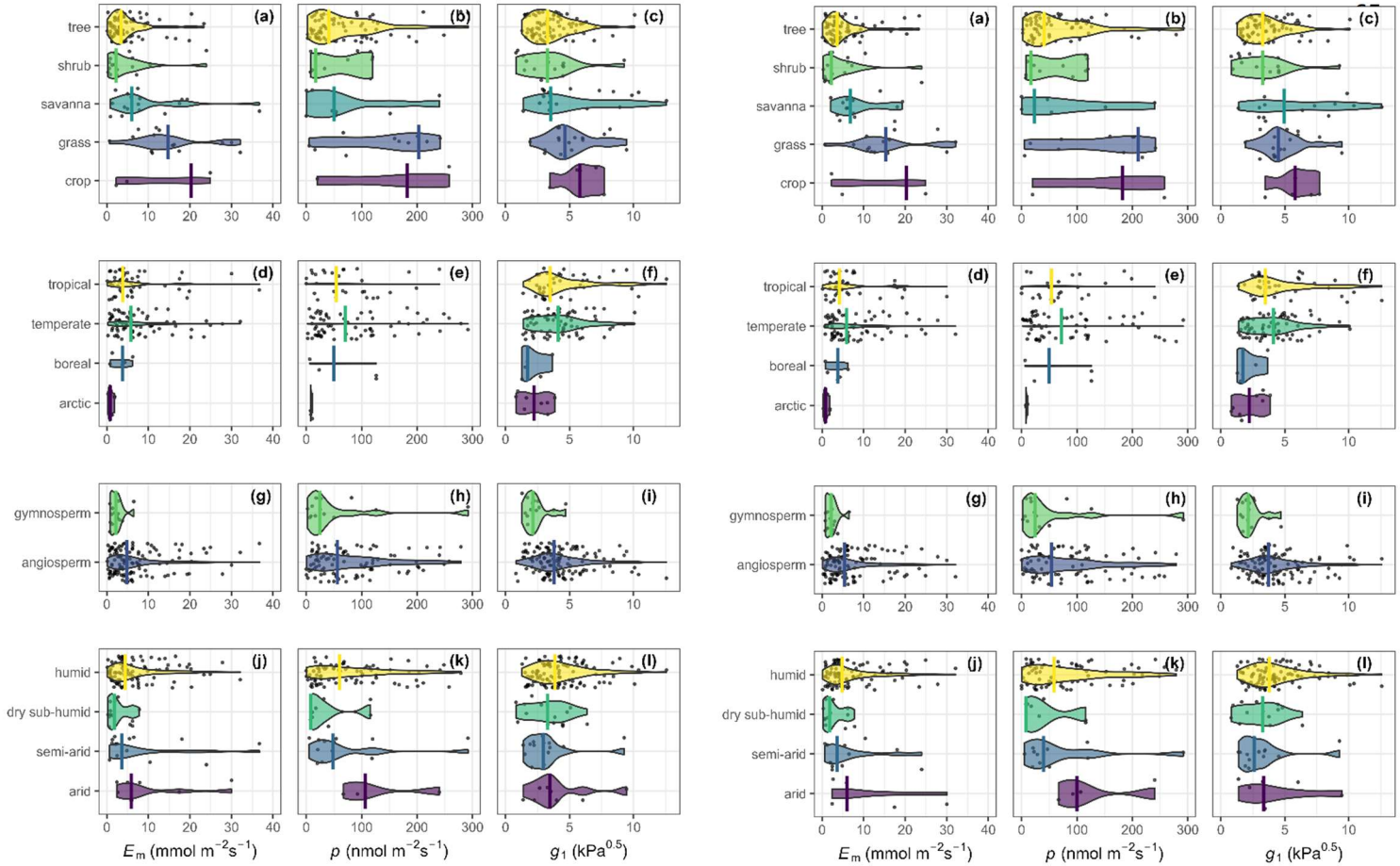

Methods S1. Derivation of solution of model for stomatal conductance with diffusional and biochemical constraints on CO_2 exchange

A. C_3 species

The model presented in this study (Eqn 3) can be written as

$$g_{sw} = \frac{E_m(B - A)}{p + (B - A)\Delta w}, \quad \text{(S1)}$$

where A is net CO_2 assimilation rate, B is CO_2-saturated assimilation rate ($A_m \equiv ¼J - R_d$, where J is potential electron transport rate and R_d is the rate of non-photorespiratory CO_2 release in the light), plus a coefficient b_o, $E_m \equiv K(\psi_s - \psi_c)$ and $p \equiv K/s$, where s is a coefficient, ψ_s is soil water potential, ψ_c is the leaf water potential at which stomata close, Δw is the leaf to air water vapor mole fraction difference, and K is leaf-specific soil-leaf hydraulic conductance. For C_3 species, the model of Farquhar et al (1980) for CO_2 assimilation rate is

$$A_v = \frac{V_m(c_i - \Gamma_*)}{c_i + K'} - R_d, \quad \text{(S2; RuBP carboxylation limited)}$$

$$A_j = \frac{J(c_i - \Gamma_*)}{4(c_i + 2\Gamma_*)} - R_d, \quad \text{(S3; RuBP regeneration limited) and}$$

$$A_t = 3 \cdot \text{TPU} - R_d, \quad \text{(S4; triose phosphate utilization limited)}$$

where A_v, A_j and A_t are carboxylation, regeneration, and triose phosphate utilization limitated values of A, V_m is the maximum carboxylation velocity, K' is the effective Michaelis constant for carboxylation ($K' = K_c(1 + O/K_o)$, where K_c and K_o are the Michaelis constants for carboxylation and oxygenation, respectively, and O is the mole fraction of oxygen), Γ_* is the photorespiratory CO_2 compensation point,

93 R_d is non-photorespiratory CO_2 release rate, J is the potential electron transport rate, and TPU is the rate
94 of triose phosphate utilization. J is modeled as a hyperbolic minimum of capacity- and light-limited rates
95 (J_m and $\phi_j i$, respectively, where i is PPFD and ϕ_j is the initial slope of J vs i), i.e., the lesser root of the
96 following quadratic expression for J:
97
98 $$\theta_j J^2 - \left(J_m + \phi_j i\right)J + J_m \phi_j i = 0 \quad \text{(S5)}$$
99
100 Note that b (= $B - A$) is given by
101
102 $$b = \tfrac{1}{4}J \cdot \frac{3\Gamma_*}{c_i + 2\Gamma_*} + b_o, \qquad (\text{S6; regeneration} - \text{limited})$$
103 $$b = \tfrac{1}{4}J - V_m\left(\frac{c_i - \Gamma_*}{c_i + K'}\right) + b_o. \ (\text{S7; carboxylation} - \text{limited})$$
104
105 *(A.i) Solution under carboxylation or regeneration-limited conditions*
106 The FvCB model under carboxylation- or regeneration-limited conditions can be expressed more
107 compactly as
108
109 $$A = \frac{W'(c_i - \Gamma_*)}{c_i + S'} - R_d = \frac{WC}{C + S}, \quad \text{(S8)}$$
110
111 where $W' \equiv V_m$ or $J/4$ and $S' \equiv K'$ or $2\Gamma_*$ under carboxylation- or regeneration-limited conditions,
112 respectively, and W, C and S are defined by
113
114 $$W \equiv W' - R_d \ , \ \text{(S9)}$$
115 $$C \equiv c_i - \Gamma \ , \ \text{(S10) and}$$

$$S \equiv S' + \Gamma\,, \quad \text{(S11)}$$

where Γ is the CO_2 compensation point (distinct from the photorespiratory CO_2 compensation point, Γ_*):

$$\Gamma \equiv \Gamma_* + \frac{R_d}{W}(\Gamma_* + S')\,. \quad \text{(S12)}$$

Solving S8 for *C* gives

$$C = \frac{SA}{W - A}\,. \quad \text{(S13)}$$

The diffusional constraint on *A*, assuming negligible boundary layer resistance, is

$$A = \frac{g_{sc}g_{bc}}{g_{sc} + g_{bc}}(c_a - c_i) = \frac{g_{sw}}{1.6 + rg_{sw}}(c_a - c_i) = \frac{g_{sw}}{1.6 + rg_{sw}}(Z - C)\,, \quad \text{(S14)}$$

where $g_{sc} = g_{sw}/1.6$ is the stomatal conductance to CO_2, g_{bc} is the boundary layer conductance to CO_2, and *r* is the boundary layer resistance to CO_2 ($1/g_{bc}$), and *Z* is defined as

$$Z \equiv c_a - \Gamma\,. \quad \text{(S15)}$$

Solving S14 for *C* gives

$$C = Z - \left(\frac{1.6}{g_{sw}} + r\right)A\,. \quad \text{(S16)}$$

Setting S13 and S16 equal and substituting S1 for g_{sw} gives

$$\frac{SA}{W-A} = Z - \left(\frac{1.6}{g_{sw}} + r\right)A = Z - rA - \frac{1.6A\left(p + \Delta w(B-A)\right)}{E_m(B-A)}\,. \quad \text{(S17)}$$

Cross-multiplying gives

$$SAE_m(B-A) = (Z-rA)E_m(B-A)(W-A) - 1.6A\left(p + \Delta w(B-A)\right)(W-A)\,. \quad \text{(S18)}$$

Expanding products and rearranging terms gives

$$[1.6\Delta w + E_m r]A^3 - \left[1.6(\Delta w(B+W) + p) + \left(S + Z + r(B+W)\right)E_m\right]A^2$$
$$+ [1.6W(\Delta wB + p) + (SB + Z(B+W) + rBW)E_m]A - ZE_mBW = 0\,. \quad \text{(S19)}$$

Eqn S19 is a cubic (3rd-order polynomial) expression for *A*:

$$q_3A^3 + q_2A^2 + q_1A + q_0A = 0\,, \quad \text{(S20)}$$

where the coefficients are given by

$$q_3 = 1.6\Delta w + E_m r\,, \quad \text{(S21)}$$

$$q_2 = -E_m\left(S + Z + r(B+W)\right) - 1.6\left(p + \Delta w(B+W)\right), \quad \text{(S22)}$$

$$q_1 = E_m(B(S+Z) + ZW + rBW) + 1.6W(p + \Delta wB)\,, \quad \text{(S23) and}$$

$$q_0 = -E_mBZW\,. \quad \text{(S24)}$$

Noting that $S + Z = c_a + S'$, Eqns S21-S24 are equivalent to A8-A11.

(A.ii) Special case #1: Regeneration-limited conditions if $b_o = 0$

Note that if $b_o = 0$, then under regeneration-limited conditions, $B = W$, which simplifies Eqn S18 to

$$SAE_m = (Z - rA)E_m(W - A) - 1.6A\big(p + \Delta w(W - A)\big) \ , \quad (S25)$$

leading to a quadratic expression for A, rather than a cubic:

$$(1.6\Delta w + E_m r)A^2 - [1.6(p + \Delta wW) + E_m(S + Z + rW)]A + ZE_mW = 0 \ . \quad (S26)$$

Thus, under these conditions, A is calculated as

$$A = \frac{1}{2q_2'}\left(-q_1' \pm \sqrt{{q_1'}^2 - 4q_0'q_2'}\right), \quad (S27)$$

where

$$q_2' \equiv 1.6\Delta w + E_m r \ , \quad (S28)$$

$$q_1' \equiv -E_m(c_a + 2\Gamma_* + rW) - 1.6(p + \Delta wW) \ , \quad (S29) \text{ and}$$

$$q_0' \equiv E_m ZW \ . \quad (S30)$$

To identify which root is correct, note that expanding Eqn S27 gives

185 $$A = \left[\frac{E_m(c_a + 2\Gamma_* + rW) + 1.6(p + \Delta wW)}{1.6\Delta w + E_m r}\right]\left(\frac{1}{2}\right.$$

186 $$\left. \pm\frac{1}{2}\sqrt{1 - \frac{4(1.6\Delta w + E_m r)E_m ZW}{\left(E_m(c_a + 2\Gamma_* + rW) + 1.6(p + \Delta wW)\right)^2}}\right). \quad \text{(S31)}$$

187

188 The quantity in square brackets is greater than *W*, whereas the quantity in large parentheses is either
189 between zero and 1/2 or between 1/2 and 1, if one chooses the smaller or larger root, respectively.
190 Choosing the larger root therefore always produces *A* > *W*/2, which is not realistic. Note as well that for
191 small Δw (low Δw), the quantity in parentheses approaches unity while that in square brackets becomes
192 much larger than *W*, such that *A* approaches a value much larger than *W*, which again is not realistic
193 because *A* cannot exceed *W*. Thus, the smaller root is the correct one.

194

195 It is not immediately obvious whether the quantity in the radical in S31 is always positive, nor therefore
196 whether the result is always real; however, it can be proven that the result is always real, as follows. In
197 order for the quantity in the radical to become negative, it first must go from being positive to being
198 zero; at the point where it is zero, the following then holds:

199

200 $$A = \frac{1}{2}\left[\frac{E_m(c_a + 2\Gamma_* + rW) + 1.6(p + \Delta wW)}{1.6\Delta w + E_m r}\right]. \quad \text{(S32)}$$

201

202 This can be rearranged to give

203

204 $$2A = \frac{\frac{E_m}{1.6\Delta w}}{1 + \frac{E_m}{1.6\Delta w}r}(c_a + 2\Gamma_*) + \frac{\frac{p}{\Delta w}}{1 + \frac{E_m}{1.6\Delta w}r} + W. \quad \text{(S33)}$$

From Eqn 5 in the main text, $E_m/\Delta w$ is the value of g_{sw} in the limit of $p \to 0$ or $b \to \infty$, meaning $g_{sw} < E_m/\Delta w$, or equivalently, $E_m/\Delta w > g_{sw}$. Note as well that $g_{sc} = g_{sw}/1.6$, so $E_m/1.6\Delta w > g_{sc}$. This inequality can be expressed as $E_m/1.6\Delta w = g_{sc} + x$, where x is some quantity greater than zero. Thus,

$$2A = \frac{g_{sc} + x}{1 + r(g_{sc} + x)}(c_a + 2\Gamma_*) + \frac{\frac{p}{\Delta w}}{1 + \frac{E_m}{1.6\Delta w}r} + W. \quad \text{(S34)}$$

The total conductance to CO_2 is $g_{tc} = g_{sc}/(1 + rg_{sc})$; but since $\partial g_{tc}/\partial g_{sc} = (1 + rg_{sc})^{-2} > 0$, it follows that $(g_{sc} + x)/(1 + r(g_{sc} + x)) > g_{tc}$, or $(g_{sc} + x)/(1 + r(g_{sc} + x)) = g_{tc} + x'$, where x' is again some quantity greater than zero. Thus,

$$2A = (g_{tc} + x')(c_a + 2\Gamma_*) + \frac{\frac{p}{\Delta w}}{1 + \frac{E_m}{1.6\Delta w}r} + W. \quad \text{(S35)}$$

The first product on the right-hand side can be rearranged as

$$(g_{tc} + x')(c_a + 2\Gamma_*) = g_{tc}(c_a - c_i) + x'(c_a - c_i) + (g_{tc} + x')(c_i + 2\Gamma_*), \quad \text{(S36)}$$

but since $g_{tc}(c_a - c_i) = A$, it follows that

$$2A = A + x'(c_a - c_i) + (g_{tc} + x')(c_i + 2\Gamma_*) + \frac{\frac{p}{\Delta w}}{1 + \frac{E_m}{1.6\Delta w}r} + W, \quad \text{(S37)}$$

or, subtracting A from both sides,

$$A = W + x'(c_a - c_i) + (g_{tc} + x')(c_i + 2\Gamma_*) + \frac{\frac{p}{\Delta w}}{1 + \frac{E_m}{1.6\Delta w} r}. \quad \text{(S38)}$$

Everything on the right-hand side to the right of W is positive (unless $c_i > c_a$, which would imply $A < 0$), so this expression implies $A > W$ if $A \geq 0$. However, W is the maximum value of A consistent with the biochemical model of photosynthesis (cf. Eqn S8), so if $A \geq 0$ ($c_i \geq c_a$), this equation represents a contradiction. If $A < 0$, then $c_i > c_a$, or equivalently, $c_i = c_a + \delta$, where $\delta > 0$, giving

$$A = W - x'\delta + (g_{tc} + x')(c_a + 2\Gamma_* + \delta) + \frac{\frac{p}{\Delta w}}{1 + \frac{E_m}{1.6\Delta w} r} \quad \text{(S39)}$$

which simplifies to

$$A = W + g_{tc}\delta + (g_{tc} + x')(c_a + 2\Gamma_*) + \frac{\frac{p}{\Delta w}}{1 + \frac{E_m}{1.6\Delta w} r} \quad \text{(S40)}$$

which again implies $A > W$. Therefore, the premise from which S40 was derived – namely, that the quantity under the radical in S31 can become negative – is not consistent with known biophysical constraints, and therefore, the radical cannot become negative and S31 always produces a real result.

(A.iii) Special case #2: Darkness (J = 0) or TPU limited conditions

In darkness or under TPU limitation, the biochemical demand expression for A is independent of c_i. For darkness, $A = -R_d$, and for TPU-limited conditions, A is given by Eqn S4. In either case, A is simply applied to Eqn S1 to calculate g_{sw}.

247

248 *(A.iv) Special case #4: $\Delta w = 0$ and $r_{bc} = 0$*

249 When $\Delta w = 0$ and $r_{bc} = 0$, the model for g_{sw} degenerates to

250

251 $$g_{sw} = E_m(B - A)/p \ , \quad (S41)$$

252

253 so that S17 is replaced with S42, which leads to a quadratic expression for A (S43):

254

255 $$\frac{SA}{W - A} = Z - \frac{1.6pA}{E_m(B - A)} \ , \quad (S42)$$

256 $$0 = -[E_m(Z + S) + 1.6p]A^2 + [E_m(B(Z + S) + ZW) + 1.6pW]A - E_m ZBW \ . \quad (S43)$$

257

258 The zeroth, first, and second order coefficients in S43 are identical to those of the original cubic solution

259 with Δw and r_{bc} set to 0, so under these conditions, one can simply compute A as

260

261 $$A = \frac{1}{2q_2}\left(-q_1 - \sqrt{q_1^2 - 4q_0 q_2}\right), \quad (S44)$$

262

263 with q_2, q_1 and q_0 found by applying $\Delta w = 0$ to Eqns S22-S24.

264

265 ***B. C_4 species***

266 In C_4 plants, the model of Collatz et al. (1992) predicts photosynthesis rate ($P = A + R_d$) from three

267 limiting conditions:

268

269 $$P_i = \alpha_c i \ , \quad (S45; \text{light} - \text{limited})$$

$$P_v = V_m \ , \quad (\mathrm{S46; capacity-limited})$$

$$P_c = k_p c_i \ , \quad (\mathrm{S47; CO_2-limited})$$

where α_c is the initial slope of A_j vs i, i is absorbed PPFD, and k_p is the initial slope of the A vs c_i curve. First, the CO_2-saturated rate, M' (note this quantity is unrelated to the net epidermal mechanical advantage, which in the main text is also symbolized as M) is computed as the hyperbolic minimum of the light- and capacity-limited rates, i.e., the lesser root M' of

$$\theta_M M'^2 - M'(V_m + \alpha_c i) + V_m \alpha_c i = 0 \ , \quad (\mathrm{S48})$$

where θ_M is a dimensionless curvature factor < 1. Then, the actual rate is computed as the hyperbolic minimum of M' and P_c, i.e., the lesser root P of

$$\beta' P^2 - P\left(M' + k_p c_i\right) + M' k_p c_i = 0 \ , \quad (\mathrm{S49})$$

where β' is a dimensionless curvature factor < 1 (unrelated to the quantity with the same symbol in the main text). To solve Eqn S49 with the diffusional constraint and the new stomatal model, first note that the latter can be written as

$$g_{sw} = \frac{(M' - R_d - A + b_o)E_m}{p + (M' - R_d - A + b_o)\Delta w} = \frac{(M'' - A)E_m}{p + (M'' - A)\Delta w} \ , \quad (\mathrm{S50})$$

where $M'' \equiv M' - R_d + b_o$. Then rearrange the diffusional constraint as $g_{sw} = 1.6A/(c_a - c_i - rA)$, and set this equal to the RHS of Eqn S50:

294 $$\frac{(M'' - A)E_m}{p + (M'' - A)\Delta w} = \frac{1.6A}{c_a - c_i - rA} \quad . \quad (S51)$$

295

296 Solving this for c_i gives

297

298 $$c_i = c_a - rA - \frac{1.6A(p + (M'' - A)\Delta w)}{(M'' - A)E_m} \quad . \quad (S52)$$

299

300 Replacing P in Eqn S49 with $A + R_d$ gives

301

302 $$\beta'(A + R_d)^2 - (A + R_d)\left(M' + k_p c_i\right) + M' k_p c_i = 0 \quad , \quad (S53)$$

303

304 and then replacing c_i in S53 with the RHS of Eqn S52 gives

305

306 $$\beta'(A + R_d)^2 - (A + R_d)\left(M' + k_p\left[c_a - rA - \frac{1.6A(p + (M'' - A)\Delta w)}{(M'' - A)E_m}\right]\right)$$

307 $$+ M' k_p\left[c_a - rA - \frac{1.6A(p + (M'' - A)\Delta w)}{(M'' - A)E_m}\right] = 0 \quad . \quad (S54)$$

308

309 Rearrangement and grouping terms leads to a cubic expression in A, with coefficients given by Eqns A12-

310 A15 in the Appendix.

311

312 ***C. Proof that there is exactly one biophysically meaningful root of the cubic solution***

313 *(i) Light-limited conditions in C_3 species*

314 When the net CO_2 assimilation rate (A) is limited by the rate of RuBP regeneration, the Farquhar model

315 for photosynthesis predicts A as

316

317 $$A = \frac{0.25J(c_i - \Gamma_*)}{c_i + 2\Gamma_*} - R_d \ . \quad \text{(S55)}$$

318

319 The diffusion constraint is

320

321 $$A = \frac{g_{sw}}{1.6 + rg_{sw}}(c_a - c_i) \ , \quad \text{(S56)}$$

322

323 where g_{sw} is stomatal conductance (≥ 0) and ambient CO_2 concentration (c_a) > 0. The new model for g_{sw}

324 is

325

326 $$g_{sw} = \frac{G(B - A)}{1 + d(B - A)}, \quad \text{(S57)}$$

327

328 where $G \equiv s(\psi_s - \psi_c)$ and $d \equiv s\Delta w/K$ are non-negative. Combining S56 and S57 and solving for c_i gives c_i as

329 a function of A:

330

331 $$c_i = c_a - \frac{[1.6(1 + dB) + rGB]A - [1.6d + rG]A^2}{G(B - A)} \equiv f_1(A) \ . \quad \text{(S58)}$$

332

333 Solving S55 for c_i gives another function relating c_i to A:

334

335 $$c_i = \frac{(2(A + R_d) + 0.25J)\Gamma_*}{0.25J - A - R_d} \equiv f_2(A) \ . \quad \text{(S59)}$$

336

Setting f_1 and f_2 equal to eliminate c_i leads to a cubic expression for A (e.g., S20). The roots of that cubic are equivalent to intersections of the functions f_1 and f_2. Our objective in this section is to show that f_1 and f_2 intersect once and only once in the region of c_i vs A space where c_i and A are biophysically meaningful, provided $J > 0$ and $c_a > \Gamma_*$ (we consider the case of $J = 0$ later). c_i cannot be lower than Γ_* (provided $c_a > \Gamma_*$), and given S55, $c_i \geq \Gamma_*$ implies $A \geq -R_d$; note that, given c_i is positive and finite, S55 also implies $A < 0.25J - R_d$. Thus, we are concerned with the topology of f_1 and f_2 subject to the constraints $-R_d \leq A < 0.25J - R_d$ and $c_i \geq \Gamma_*$. The derivatives of f_1 and f_2 with respect to A are

$$\frac{\partial f_1}{\partial A} = -r - 1.6\frac{B + d(B-A)^2}{G(B-A)^2} \quad , \qquad \text{(S60)}$$

and

$$\frac{\partial f_2}{\partial A} = \frac{3\Gamma_* J}{4(0.25J - R_d - A)^2} \quad . \quad \text{(S61)}$$

$\partial f_2/\partial A$ is strictly positive if $J > 0$, and $\partial f_1/\partial A$ is strictly negative if $B \geq 0$. We will consider the case where $B < 0$ separately, later. The value of f_1 at the lower limit of the interval of interest ($A = -R_d$) is

$$f_1(-R_d) = c_a + \frac{R_d\big(1.6 + (1.6d + rG)(B + R_d)\big)}{G(B + R_d)} \quad . \quad \text{(S62)}$$

Since $B + R_d = 0.25J + b_o$, and by premise $J > 0$, $b_o \geq 0$, $d \geq 0$ and $G > 0$, and given $R_d \geq 0$ by definition, it follows that $B + R_d \geq 0$ and therefore $f_1(-R_d) \geq c_a$. The value of f_2 at $A = -R_d$ is

$$f_2(-R_d) = \Gamma_* \ . \quad \text{(S63)}$$

Thus, since $c_a > \Gamma_*$ by premise, it follows that $f_1(-R_d) > f_2(-R_d)$. The value of f_1 at the upper boundary of the domain of interest ($A = 0.25J - R_d$) is a finite number if $b_o > 0$:

$$f_1(0.25J - R_d) = c_a - (0.25J - R_d)\frac{1.6 + (1.6d + rG)b_o}{Gb_o} \ , \quad \text{(S64)}$$

and the limit of f_1 as A approaches $0.25J - R_d$ from below is minus infinity if $b_o = 0$:

$$\lim_{A \to 0.25J - R_d} f_1(A) = -\infty \ . \quad \text{(S65)}$$

f_2 approaches positive infinity as A approaches $0.25J - R_d$ from below for $J > 0$:

$$\lim_{A \to 0.25J - R_d} f_2(A) = +\infty \ . \quad \text{(S66)}$$

Thus, provided $J > 0$ and $B \geq 0$, we have four facts: (i) $f_2 < f_1$ at the lower limit of the valid domain for A, (ii) $f_2 > f_1$ at the upper limit of that domain, (iii) f_2 increases monotonically with increasing A, and (iv) f_1 decreases monotonically with increasing A. Given these facts, then by the Intermediate Value Theorem, f_1 and f_2 must intersect exactly once at some point in the domain; equivalently, exactly one of the cubic roots occurs in the biophysically meaningful domain. This means that any root found to be valid must

also be the correct one, which leads to a simple algorithm: obtain roots in turn, each time computing the implied values of A and c_i, and accept the first root for which $A \in [-R_d, 0.25J - R_d]$ and $c_i > \Gamma_*$.

If $B < 0$ (which only occurs in very low light), the situation is more complicated. First, note that the continuity of f_1 and f_2 in the interval, together with the facts that $f_2 < f_1$ at the lower end of the interval and $f_2 > f_1$ at the upper end, proves the existence of *at least one* intersection in the interval. However, note that the right segment of f_1 (for $A > B$) is also non-monotonic, and goes from $-\infty$ to a positive value greater than c_a and back to $-\infty$ again as A varies from B to $+\infty$. By contrast, f_2 is monotonic, $\partial f_2/\partial A > 0$ in that domain, and f_2 approaches $-2\Gamma_*$ as A approaches $+\infty$. Moreover, if $b_o > 0$, the value of f_2 is finite at $A = B$. Therefore, the right segment of f_1 must cross f_2 twice in the interval $B \le A < +\infty$. Since we know there are no more than three real roots, it follows that no more than one root can occur *outside* that interval (i.e., for $A < B$), and therefore, nore more than one root can occur in the biophysically meaningful domain ($-R_d \le A < B$). Yet we know that one root *must* occur in that domain (given the continuity of f_1 and f_2 and the fact that $f_2 < f_1$ at the start and $f_2 > f_1$ at the end of the interval), so there must be exactly one biophysically meaningful root, and hence any biophysically meaningful root must be the correct one.

If $b_o = 0$ under regeneration-limited conditions, then as discussed earlier, the cubic degenerates to a quadratic and the solution is given by the lesser root in Eqn S27.

(ii) Carboxylation-limited conditions in C_3 species

When the assimilation rate is limited by the rate of RuBP carboxylation in C_3 plants, Eqn S55 is replaced with

$$A = \frac{V_m(c_i - \Gamma_*)}{c_i + K'} - R_d \ , \quad (S67)$$

and the upper limit for A is $V_m - R_d$ instead of $0.25J - R_d$. Thus, at first it seems we are concerned with the topology of f_1 and f_2 subject to the constraints $c_i > \Gamma_*$ and $-R_d \le A < V_m - R_d$. However, values of A exceeding B are not biophysically meaningful, because they would imply $g_{sw} < 0$ in the stomatal conductance model. Thus, the interval of interest for A is actually $-R_d \le A < B$, unless it happens (though it is unlikely) that $V_m - R_d < B$ (recall $B \equiv J/4 - R_d + b_o$), in which case the intervals ends at $V_m - R_d$. We will consider each case in turn below.

Under carboxylation limited conditions, the expression for f_2 (Eqn S59) is replaced with

$$c_i = \frac{K'(A + R_d) + V_m\Gamma_*}{V_m - (A + R_d)} \equiv f_2(A) \ , \quad (S68)$$

but the expression for f_1 is unchanged (because B always equals $0.25J - R_d + b_o$ for C_3 species in the model for stomatal conductance, regardless of which limiting condition for photosynthesis is being considered):

$$c_i = c_a - \frac{[1.6(1 + dB) + rGB]A - [1.6d + rG]A^2}{G(B - A)} \equiv f_1(A) \ . \quad (S69)$$

Setting f_1 and f_2 equal to eliminate c_i leads to a cubic expression as before. The derivatives of f_1 and f_2 are

$$\frac{\partial f_1}{\partial A} = -r - 1.6\frac{B + d(B-A)^2}{G(B-A)^2} \quad . \quad \text{(S70)}$$

$\partial f_1/\partial A$ is strictly negative if $B \geq 0$, and strictly positive if $B < 0$.

$$\frac{\partial f_2}{\partial A} = \frac{V_m(K' + \Gamma_*)}{(V_m - R_d - A)^2} , \quad \text{(S71)}$$

which is strictly positive for $V_m - R_d - A \neq 0$ because $V_m > 0$. Now we need to consider the values of f_1 and f_2 at each end of the interval. As we found under regeneration-limited conditions, the value of f_1 at the lower limit of the interval ($A = -R_d$) is

$$f_1(-R_d) = c_a + \frac{R_d\big(1.6 + (1.6d + rG)(B + R_d)\big)}{G(B + R_d)} \quad , \qquad \text{(S72)}$$

so again we have $f_1(-R) \geq c_a$. The value of f_2 at $A = -R_d$ is also again Γ_*:

$$f_2(-R_d) = \Gamma_* \quad \text{(S73)}$$

so as before, $f_1 > f_2$ at the lower end of the interval of interest. For the upper end of the interval, however, we must consider three scenarios: Case #1 ($V_m - R_d > B$, so the upper end of the interval is $A = B$), Case #2 ($V_m - R_d = B$, so the upper end of the interval is $A = B = V_m - R_d$), and Case #3 ($V_m - R_d < B$, so the upper end of the interval is $A = V_m - R_d$). In Cases #1 and #2, as A approaches the upper end of the interval (B) from below, f_1 approaches minus infinity (provided $B > 0$):

$$\lim_{A \to B} f_1(A) = -\infty \quad \text{(S74)}$$

In Case #3, the value of f_1 at the upper end of the interval ($V_m - R_d$) is

$$c_a - (V_m - R_d)\frac{1.6 + (1.6d + rG)(B - V_m + R_d)}{G(B - V_m + R_d)} \ , \quad \text{(S75)}$$

which is a positive number less than c_a (because $B > V_m - R_d$ by premise in Case #3). Now we consider f_2. In Case #1, the value of f_2 at the upper end of the interval ($A = B$) is

$$f_2(B) = \frac{K'(B + R_d) + V_m\Gamma_*}{V_m - R_d - B} = \frac{K'(B + R_d)}{V_m - R_d - B} + \frac{V_m}{V_m - R_d - B}\Gamma_* \quad \text{(S76)}$$

which is a positive number greater than Γ_* because $V_m - R_d > B$ by premise in Case #1. In Case #2, f_2 approaches positive infinity as A approaches the upper end of the interval (B):

$$\lim_{A \to B} f_2(A) = +\infty \quad \text{(S77)}$$

In Case #3, f_2 again approaches positive infinity as A approaches the upper end of the interval ($V_m - R_d$):

$$f_2(V_m - R_d) = \frac{K'\big((V_m - R_d) + R_d\big) + V_m\Gamma_*}{V_m - \big((V_m - R_d) + R_d\big)} \quad \text{(S78)}$$

Thus, in each case, and given $B \geq 0$, we again have the four required premises for the Intermediate Value Theorem to prove that there is exactly one intersection between f_1 and f_2 within the interval: $\partial f_1/\partial A$ is strictly negative in the interval, $\partial f_2/\partial A$ is strictly positive, $f_1 > f_2$ at the lower end of the interval, and $f_1 < f_2$ at the upper end of the interval.

(iii) When B < 0 in C_3 species

If $B < 0$, again we need to consider each case separately. In Case #1, the interval ends at $A = B$, so f_1 approaches positive infinity at the upper end of the interval. However, in this case f_2 does not approach positive infinity within the interval. Since $f_1 > f_2$ at both the beginning and end of the interval, it follows that f_1 and f_2 do not necessarily intersect in the interval. They must intersect at least twice in the interval for $A > B$, because f_2 is finite at the bottom of that interval, is monotonic, and approaches $+\infty$ somewhere in the interval, whereas f_1 rises from $-\infty$ as A increases from B and falls again to $-\infty$. The right-hand segment of f_2 rises from $-\infty$ at $A = V_m - R_d$ and eventually approaches $-K'$, and therefore crosses f_1 once. Thus, in this case, all three intersections are in the biophysically non-meaningful domain, which means the algorithm must include an option for "no solution", returning NA or similar for each variable in the model.

(iv) C_4 species

The analogue of Eqn S58 for C4 species is Eqn S52, reproduced here:

$$c_i = c_a - \frac{A\left(1.6p + (M'' - A)(1.6\Delta w + rE_m)\right)}{(M'' - A)E_m} \equiv f_3(A) \quad , \quad \text{(S79)}$$

and the analogue of S59 is

$$c_i = \frac{(A + R_d)(M' - \beta' R_d - \beta A)}{k_p(M' - R_d - A)} = \frac{(A + R_d)}{k_p}\left(1 + \frac{\beta'(A + R_d)}{(M' - R_d - A)}\right) \equiv f_4(A) \quad . \quad \text{(S80)}$$

Our objective again is to prove that f_3 and f_4 intersect exactly once under biophysically meaningful conditions. We exclude here conditions where $M' = 0$, because A is simply R_d in that case. First, it is clear by inspection that f_4 is a monotonically increasing function of A. Second, its values at the lower and upper ends of the relevant range ($A = -R_d$ and $M' - R_d$, respectively) are zero and $+\infty$, respectively. The derivative of f_3 with respect to A is

$$\frac{\partial f_3}{\partial A} = -\frac{1.6pM'' + (1.6\Delta w + rE_m)(M'' - A)^2}{(M'' - A)^2 E_m} \quad , \quad \text{(S81)}$$

which is always negative for $M' > 0$ (because $M'' - A = M' - P + b_o$, and $M' > P$ if $M' > 0$); thus, f_3 is a monotonically decreasing function of A. The value of f_3 at the lower end of the range is

$$f_3(-R_d) = c_a + \frac{R_d\left(1.6p + (M'' + R_d)(1.6\Delta w + rE_m)\right)}{(M'' + R_d)E_m} \quad , \quad \text{(S82)}$$

which is larger than c_a, so $f_3 > f_4$ at the lower end of the interval. Since $f_4 \rightarrow \infty$ at the upper end of the interval and f_3 is monotonically decreasing, $f_3 < f_4$ at the upper end of the interval. Since both f_3 and f_4 are monotonic, it follows by the Intermediate Value Theorem that they intersect exactly once in the interval, and hence there is exactly one meaningful root to the cubic in C_4 species.

Methods S2. Derivation of cubic solution for USO model when $r_{bc} > 0$ and $g_0 > 0$

For application to Dataset #3, in which whole-plant gas exchange rates are of significant interest, it was necessary to account for boundary layer resistance when computing assimilation and transpiration rates from either the new model or the USO model. For the latter, including $r_{bc} > 0$ leads to a cubic solution, rather than the usual quadratic or linear solutions (when $g_0 > 0$ or $g_0 = 0$, respectively). We derive the cubic form here.

Define $x \equiv 1.6(1 + g_1/D^{0.5})/c_a$, such that the USO model is given by

$$g_{sw} = xA + g_0 \,. \quad \text{(S83)}$$

From Eqn S13, the leaf-air CO_2 gradient, $c_a - c_i = Z - C$ is given by

$$Z - C = Z - \frac{SA}{W - A} = \frac{ZW - (Z + S)A}{W - A} \,, \quad \text{(S84)}$$

in which Z, C, W and S depend on whether photosynthesis is carboxylation or regeneration limited, and are defined in Methods S1(A.i). The diffusion constraint with $r_{bc} > 0$ is given by S14, which combines with S84 to give

$$A = \frac{g_{sw}}{1.6 + r_{bc} g_{sw}} \frac{ZW - (Z + S)A}{W - A} \,. \quad \text{(S85)}$$

Applying Eqn S83 gives

$$A = \frac{xA + g_0}{1.6 + r_{bc}g_0 + r_{bc}xA}\frac{ZW - (Z + S)A}{W - A}\,. \quad \text{(S86)}$$

Multiplying through by the denominator of the right-hand side gives

$$A(W - A)(1.6 + r_{bc}g_0 + r_{bc}xA) = (xA + g_0)(ZW - (Z + S)A)\,. \quad \text{(S87)}$$

Expanding this expression and grouping terms by order gives a cubic expression for *A*:

$$q_3A^3 + q_2A^2 + q_1A + q_0A = 0\,, \quad \text{(S88)}$$

where the coefficients are given by

$$q_3 = -r_{bc}x\,, \quad \text{(S89)}$$

$$q_2 = -(1.6 + r_{bc}g_0) + r_{bc}xW + x(Z + S)\,, \quad \text{(S90)}$$

$$q_1 = W(1.6 + r_{bc}g_0) - xZW + g_0(Z + S)\,, \quad \text{(S91) and}$$

$$q_0 = -g_0ZW\,. \quad \text{(S92)}$$

If $g_0 = 0$ but $r_{bc} > 0$, this reduces to a quadratic expression for *A*, in which the 2nd, 1st and zeroth-order coefficients are given by S89, S90, and S91, respectively.

Methods S3. Description of datasets used for validation of the new model, and associated calculations

A. Dataset #1: diurnal measurements in grapevine, olive and almond under control and drought conditions (Figure 2 in the main text)

Almond plants were two-year-old individuals grown from seed in 50 L pots outdoors near Sevilla, olive plants were 6-year old trees growing in the natural soil of the same site as the almond experiment, and grapevine plants were 3-year-old vines growing in natural soil in a field site near the University of Balearic Islands, Spain. All species were drip-irrigated. Almond plants were irrigated to keep soil water content near field capacity (control) or to reduce soil water content by 69% (drought). Olive plants were irrigated by an amount estimated from meteorological conditions (control), or deficit irrigated to 30% of that value (drought). Grapevines were irrigated to keep soil water potential (estimated as predawn leaf water potential) between -0.3 and -0.4 MPa (control) or not irrigated at all throughout the summer (drought).

Air temperature and relative humidity, from which Δw was calculated, were measured near the almond plants using ZIM probes, and for the olive and grapevine plants, using meteorological stations placed in the same fields as the plants. Predawn and midday leaf water potentials ($\psi_{leaf,pd}$ and $\psi_{leaf,md}$, respectively) were measured with a Scholander pressure chamber. Stomatal conductance was measured periodically (every 1.5 to 3 hours) with an Li-6400 (Li-Cor, Lincoln, NE) with PPFD and temperature set to match ambient conditions, chamber CO_2 set to 390-400 ppm (close to the prevailing atmospheric value in 2012, when the experiment was conducted), and the chamber oriented to match the original leaf orientation, and the PPFD measured by the Li-6400's quantum sensor was recorded. g_{sw} was measured within 1-2 minutes of enclosing the leaf in the chamber.

We fitted the parameters ψ_c, s and b_o to each dataset, either separately for the two treatments in a given species (giving separate parameter sets for each treatment), or together (giving a single parameter set for both treatments), using the function *optim* in R (using the Nelder-Mead algorithm). K was calculated from predawn and midday leaf water potential and midday stomatal conductance and Δw as $K = g_{sw} \cdot \Delta w / (\psi_{leaf,pd} - \psi_{leaf,md})$ for each plant, and corrected for midday temperature to obtain K_{25}. Photosynthetic parameters and their temperature responses were measured and estimated separately in each treatment for each species, as previously described (Rodriguez-Dominguez et al., 2016).

B. Dataset #2: diurnal gas exchange under combined drought and heat stress (Figure 3 in the main text)

To compare the new model's ability to predict gas exchange under combined drought and heat stress with that of the USO model, we conducted simulations of published measurements of whole tree gas exchange in potted seedlings of *Eucalyptus parramattensis* (Drake et al., 2018), for which soil water was withheld for one month and then heatwaves were imposed. Heatwaves consisted of four sunny days with maximum diurnal air temperature at 43-44°C and VPD of 5-6 kPa; for the control, maximum diurnal air temperature was set at 28-29°C. The heatwave was imposed on 2016-10-30. Measurements were reported for six trees each in the control and heatwave treatment; of the six trees in each treatment, three had been subjected to a long-term mild warming treatment of ambient +3°C for one year prior to the heatwave (beginning on 2015-10-28), while the other three had been set to track ambient temperature. Following Drake et al. (2018), we pooled data across the six trees within the heatwave treatment, and within the control treatment (i.e., not distinguishing the long-term mild warming treatment). To drive the stomatal models, we used environmental conditions and photosynthetic parameters and temperature responses reported by Sicangco et al. (2026) for the experiment. For comparison with measured fluxes, we calculated leaf net CO_2 assimilation rate (A) directly, in the course of predicting g_{sw} for each model, and leaf transpiration rate (E) as

608

609 $$E = \frac{g_{sw}}{1 + r_{bw} g_{sw}} \Delta w \,, \quad \text{(S93)}$$

610

611 in which r_{bw} is the boundary layer resistance to water vapor. We calculated r_{bw} as the inverse of the

612 boundary layer conductance to water vapor, g_{bw}, which in turn was calculated following Leuning et al.

613 (1995) from the sum of forced and free components of the boundary layer condcutance to sensible heat

614 (g_{bhw} and g_{bhf}, respectively), given by

615

616 $$g_{bhw} = 0.003 \cdot \frac{P_{atm}}{R_{gas} T_{airK}} \left(\frac{v_{wind}}{d_{leaf}} \right)^{0.5} \,, \quad \text{(S94)}$$

617

618 (in which P_{atm} [Pa] is atmospheric pressure, R_{gas} = 8.31446 Pa m^3 mol^{-1} K^{-1}, T_{airK} is air temperature in

619 kelvins, v_{wind} is wind speed in m s^{-1} [not provided by Drake et al. 2018 or Sicangco et al. 2026, but cited as

620 5 m s^{-1} in public code associated with the latter paper [https://github.com/CamilleSicangco/weighing-

621 the-options], and d_{leaf} is leaf width in m [given by Sicangco et al as 0.025 m]), and

622

623 $$g_{bhf} = 0.5 D_h \cdot \frac{P_{atm}}{R_{gas} T_{airK}} \cdot \left[\frac{1.6 \cdot 10^8 \cdot \left| T_{leafC} - T_{airC} \right|}{d_{leaf}} \right]^{0.25} \,, \quad \text{(S95)}$$

624

625 in which D_h is the diffusion coefficient for heat (2.15·10^{-5} m^2 s^{-1}). $g_{bh} = g_{bhw} + g_{bhf}$, and $g_{bw} = g_{bh}/1.075$

626 (Leuning et al. 1995). g_{bw} thus calculated was between 1.549 and 1.957 mol m^{-2} s^{-1} across the dataset.

627 Finally, we calculated canopy A (A_c) and transpiration (E_c) as A/2.9 and E/2.9, respectively (2.9 [unitless]

628 was the leaf-to-canopy scaling factor given by Sicangco et al. 2026).

629

We extracted measured *A* and *E*, and predictions from the USO model, from the dataset accompanying Sicangco et al. (https://github.com/CamilleSicangco/weighing-the-options/tree/main/data/out/, files control_runs.Rdata and heatwave_runs.Rdata). For the new model, we followed Sicangco et al. in accounting for hydraulic vulnerability by using their vulnerability curve ($K_{25}(\psi)/K_{25max} = f_v(\psi) = \exp(-(\psi/-4.492)^{3.713})$) and computing flow rate by integrating along the transpiration stream (water flux = $K_{25\max} f_T(T_K) \int_{\psi_s}^{\psi_L} f_v(\psi) d\psi$); in these expressions, K_{25} is the value of *K* at a given ψ and 25°C, K_{25max} is the value at ψ = 0 and 25°C, and $f_T(T_K)$ is the correction for the temperature dependence of water viscosity ($f_T(T_K) = [4.891 \cdot 10^{10} \cdot \exp(-4209/T_K - 0.04527 \cdot T_K + 3.376 \cdot 10^{-5} \cdot T_K^2)]$, where T_K is air temperature in kelvins). We used function trapz() in R package pracma to numerically integrate the vulnerability curve, with 500 steps. To compute soil-leaf *K* to apply to the new model, we then divided the resulting water flux by the gradient ($\psi_s - \psi_L$). These calculations required knowing the endpoint of integration, i.e., ψ_L, which in turn depended on the output of the model itself; thus, we solved the model by numerical iteration, by minimizing the squared difference between 'input' ψ_L (used to compute *K* from the vulnerability curve) and 'output' ψ_L (predicted by the model, given *K*), using function optimize() in R, with default settings and search bounds given by -5.5 MPa (the value of ψ_L causing 88% loss of conductivity, reported by Sicangco et al.) and ψ_s. We adjusted the parameters *s*, K_{25}, and ψ_c by hand to minimize the sum of squared errors between observed and predicted *E* for the control trees (having found that none of the algorithms available in R provided a satisfactory fit). The final parameter values were *s* = 0.06 mol^2 m^{-2} s^{-1} μmol^{-1} MPa^{-1}, ψ_c = -1.77 MPa, and K_{max25} = 4.0 mmol m^{-2} s^{-1} MPa^{-1}. For comparisons of ψ_L predicted by the USO model and the new model in this dataset, we calculated USO-predicted ψ_L as $\psi_L = \psi_s - E_{USO}/K$, where E_{USO} was the transpiration rate predicted by USO and *K* was the value computed within our own model as described earlier; this was necessary because Sicangco et al. found a much lower value of K_{25max} (1.5 mmol m^{-2} s^{-1} MPa^{-1}) from fitting HP-type stomatal models to their dataset, so applying their *K* values would unfairly bias USO-predicted ψ_L to very low values (e.g., Figure 8 in Sicangco et al.).

C. Dataset #3: Lin et al 2015 survey data (Figure 5 in the main text)

This dataset comprised in situ measurements of g_{sw}, A, VPD, c_a, and leaf temperature for 314 species in 55 sites (336 species × site combinations); we used a subset of this dataset (selected as described below), comprising 133 species in 53 sites (140 species × site combinations). To apply these data to our model, it was necessary to estimate Δw from VPD, and to estimate the residual photosynthetic capacity. Given that Δw is VPD divided by atmospheric pressure, which was not reported by Lin et al., we used the coordinates given for each site to estimate site elevation (method *get_point_elevation*() in R package *elevatr*), and calculated pressure in kPa as $101.325 \cdot ((1 - 2.25577 \cdot 10^{-5} \cdot \{\text{elevation/m}\})^{5.25588}$ (National Oceanic and Atmospheric Administration et al., 1976).

To estimate the residual photosynthetic capacity, one normally requires a full set of parameters for the relevant biochemical photosynthesis model, which were not available in the Lin dataset. Alternatively, if one assumes photosynthesis is light-limited, then one can estimate residual photosynthetic capacity (which for C_3 species equals $0.25J - R_d - A$) solely from A and c_i for C_3 species, as follows. Under regeneration-limited conditions, Eqn S3 implies $A_m - A = (A + R_d) \cdot 3\Gamma_*/(c_i - \Gamma_*)$; assuming $b_o = 0$ and $A \gg R_d$, it follows that $b \approx A \cdot 3\Gamma_*/(c_i - \Gamma_*)$. We thus estimated b for C_3 species by applying measured A to this expression, with Γ_* estimated from temperature following Bernacchi et al. (2001) (assuming 25°C if T was not reported) and c_i estimated from measured A and g_{sw} as $c_i = c_a - 1.6A/g_{sw}$.

We fitted both the USO model (Eqn 2) and the new model (in the form given by Eqn 5) to the data for each species × site combination using method nls() in R, adjusting the parameter g_1 in the USO model and the parameters E_m and p in the new model.

678 The function nls() requires initial guesses for fitted parameters. For the USO model, we inverted Eqn 2 to
679 give $g_1 = (g_{sw}c_a/(1.6A) - 1)\cdot D^{0.5}$, applied measured values of g_{sw}, c_a, A and D to this expression, and used
680 the mean of the result for each species × site combination as an initial guess for g_1. For Eqn 5, we used
681 the maximum value of E ($g_{sw}\cdot\Delta w$) for each species × site combination as an initial guess for E_m, and for p,
682 we used the mean value of b times 20/3[1]. In 15 of 140 cases, nls() could not find a solution using those
683 initial parameter estimates for E_m and p. In those cases, we inverted Eqn 5 to give $r_{sw} = (1/g_{sw}) =$
684 $(1/E_m)\cdot\Delta w + (p/E_m)\cdot(1/b)$, used lm() to fit r_{sw} as a linear function of Δw and $1/b$, extracted E_m and p from
685 the resulting fitted slopes, and applied them as initial estimates for nls(). This resolved the problem in
686 two cases. For the remaining 13 points, we simply retained the estimates of E_m and p from the linear fit.
687 Figure S2 shows results including those 13 points (as shown in Figure 5 in the main text), or excluding
688 them; the results are qualitatively identical, suggesting that using the linear fits does not introduce a
689 fundamental bias.
690
691 The original dataset contained 15,162 sets of measurements ('rows') in 314 species in 55 sites (336
692 species × site combinations). However, we excluded some rows, for two reasons. First, we excluded C_4
693 species, because r cannot be estimated in C_4 species using the data available in the Lin dataset. Second,
694 we excluded 40 rows for which intercellular CO_2 concentration (calculated from the reported A and g_{sw})
695 was below $\Gamma*$ in C_3 species, because this is impossible at steady-state unless $c_a < \Gamma*$ and $A < 0$ (conditions
696 that were not met). Third, to avoid overfitting, we excluded species × site combinations for which fewer

[1] $p \approx \langle b\rangle\cdot 20/3$ arises from the meta-analysis of stomatal responses to Δw by Oren et al. (1999), who found that the sensitivity of g_{sw} to relative changes in Δw ($\partial g_{sw}/\partial\ln[\Delta w/\Delta w_{ref}]$, where Δw_{ref} is a reference value of 10 mmol mol^{-1}) was proportional to the value of g_{sw} itself at Δw_{ref}, by a factor 0.6 (that is, $\partial g_{sw}/\partial\ln[\Delta w/\Delta w_{ref}] = 0.6\cdot g_{sref}$). Buckley et al. (2012) showed that, in the context of the BMF model, which can be written in a form identical to the new model, the Oren result implied that $p/b_{ref} = (2/3)\cdot\Delta w_{ref}$, where b_{ref} is the value of b that obtains when $\Delta w = \Delta w_{ref}$. Given Δw_{ref} = 10 mmol mol^{-1}, this leads to $p \approx (20/3)\cdot b_{ref}$.

than four measurements were available. This left a total of 13,736 rows, representing 133 species in 53 sites, with a total of 140 species × site combinations.

D. Dataset #4: light-response curves measured by Lamour et al. 2022 (Figure 6 in the main text)

To test whether the new model can reproduce a linear relationship between predicted and measured g_{sw} for light response curves, or if instead the predictions systematically deviate in the negative direction from observations at high PPFD, like the USO model (Lamour et al., 2022) (hereafter 'L22'), we fitted both models to measurements of responses of g_{sw} to PPFD for three tropical tree species (*Brosimum utile* [Kunth] Oken, *Cecropia insignis* Liebm. and *Guatteria dumetorum* R.E.Fr.), for 10, 9 and 7 leaves per species, respectively, using measurements of carboxylation capacity at 25°C (V_{m25}), electron transport capacity at 25°C (J_{m25}), and leaf respiration rate at 25°C (R_{d25}) made by the same authors on different leaves of the same species and in the same canopy locations, and environmental conditions used in the leaf chamber during g_{sw} vs PPFD response curves; fitting was done using optim() in R, with the L-BFGS-B algorithm. Leaf temperature was held constant for each leaf (at values between 28 and 32°C) and Δw was held approximately constant, varying by an average of 1.1 mmol mol^{-1} within each response curve, around modal values that varied between 5 and 21 mmol mol^{-1} among leaves, depending on ambient conditions. Additional details about the trees and measurements are available in L22. We assumed the curvature parameter (θ_J) and initial slope (ϕ_J) for the response of potential electron transport rate (J) to light were equal to those measured by L22 for assimilation rate.

Methods S4. Additional details of simulations using the new model

Except for Dataset #1 (where species-specific temperature responses were provided by the original authors), we used expressions given by Bernacchi et al (C. Bernacchi et al., 2003; C. J. Bernacchi et al., 2001) to predict temperature responses for photosynthetic parameters (V_m, J_m, Γ_*, K', ϕ_j, θ_j and R_d):

$$V_m = V_{m25} \cdot \exp\left(26.35 - \frac{65.33}{R_{gas}T_{leafK}}\right), \quad \text{(S96)}$$

$$J_m = J_{m25} \cdot \exp\left(17.7 - \frac{43.9}{R_{gas}T_{leafK}}\right), \quad \text{(S97)}$$

$$\Gamma_* = \exp\left(19.02 - \frac{37.83}{R_{gas}T_{leafK}}\right), \quad \text{(S98)}$$

$$K_c = \exp\left(38.05 - \frac{79.43}{R_{gas}T_{leafK}}\right), \quad \text{(S99)}$$

$$K_o = \exp\left(20.3 - \frac{36.38}{R_{gas}T_{leafK}}\right), \quad \text{(S100)}$$

$$\phi_j = 0.5\left(0.352 + 0.022T_L - 0.00034T_{leaf}^2\right), \quad \text{(S101)}$$

$$\theta_j = 0.76 + 0.018T_L - 0.00037T_{leaf}^2, \quad \text{(S102)} \quad \text{and}$$

$$R_d = 0.01V_{m25} \cdot \exp\left(18.72 - \frac{46.39}{R_{gas}T_{leafK}}\right), \quad \text{(S103)}$$

where T_{leaf} and T_{leafK} are leaf temperature in degrees C and kelvins, respectively, R_{gas} is the gas constant (0.00831446).

As with the optimization-based model of Cowan and Farquhar (1977), the current model's predictions are often discontinuous at the point corresponding to the transitions among carboxylation,

738 regeneration, or TPU limitation. This discontinuity is an artefact of the biochemical model's assumption
739 that photosynthesis at the leaf scale is entirely limited by only one of these factors. In reality, given
740 transdermal gradients of light and photosynthetic capacity, it is unlikely that all chloroplasts in a leaf will
741 simultaneously shift between transitions (Badeck, 1995; Buckley & Farquhar, 2004), such that transitions
742 at the whole-leaf scale will generally be more gradual. To account for realistic "co-limitation" of leaf-
743 scale photosynthesis by multiple factors, we used a non-rectangular hyperbola to 'smooth' transitions
744 (Eqn S104).
745

746 $$A = \frac{1}{2\theta_A}\left(A_v + A_j - \sqrt{\left(A_v + A_j\right)^2 - 4\theta_A A_v A_j}\right) \quad \text{(S104)}$$

747

748 where A_v and A_j are the rates of photosynthesis limited by carboxylation and regeneration, respectively,
749 and θ_A is a dimensionless factor close to unity that controls the degree of smoothing. θ_A = 1 corresponds
750 to a simple minimum, i.e., $A = \min\{A_v, A_j\}$, and values below 1 are smoothed; we used θ_A = 0.99 for
751 simulations unless otherwise noted, to achieve a degree of realistic smoothing without artefactually
752 reducing *A* (cf. Figure 3 in Buckley et al., 2017). A similar procedure can also be used to smooth the
753 transition between limitation by the supply of triose phosphate (A_v or A_j) and its utilization. Smoothing
754 the transitions in this way before applying *A* to Eqn 3 eliminates the discontinuous predictions.
755
756

References

Badeck, F.-W. (1995). Intra-leaf gradient of assimilation rate and optimal allocation of canopy nitrogen: A model on the implications of the use of homogeneous assimilation functions. *Australian Journal of Plant Physiology*, *22*, 425–439.

Bernacchi, C. J., Singsaas, E. L., Pimentel, C., Portis, A. R. J., & Long, S. P. (2001). Improved temperature response functions for models of Rubisco-limited photosynthesis. *Plant, Cell and Environment*, *24*, 253–259.

Bernacchi, C., Pimentel, C., & Long, S. P. (2003). In vivo temperature response functions of parameters required to model RuBP-limited photosynthesis. *Plant, Cell & Environment*, *26*(9), 1419–1430.

Buckley, T. N., & Farquhar, G. D. (2004). A new analytical model for whole-leaf potential electron transport rate. *Plant, Cell and Environment*, *27*, 1487–1502.

Buckley, T. N., Sack, L., & Farquhar, G. D. (2017). Optimal plant water economy. *Plant, Cell & Environment*, *40*(6), 881–896.

Buckley, T. N., Turnbull, T. L., & Adams, M. A. (2012). Simple models for stomatal conductance derived from a process model: Cross-validation against sap flux data. *Plant, Cell & Environment*, *35*(9), 1647–1662. https://doi.org/10.1111/j.1365-3040.2012.02515.x

Collatz, G. J., Ribas-Carbo, M., & Berry, J. A. (1992). Coupled photosynthesis-stomatal conductance model for leaves of C4 plants. *Functional Plant Biology*, *19*(5), 519–538.

Cowan, I. R., & Farquhar, G. D. (1977). Stomatal function in relation to leaf metabolism and environment. *Symposium of the Society for Experimental Biology*, *31*, 471–505.

Drake, J. E., Tjoelker, M. G., Vårhammar, A., Medlyn, B. E., Reich, P. B., Leigh, A., Pfautsch, S., Blackman, C. J., López, R., & Aspinwall, M. J. (2018). Trees tolerate an extreme heatwave via sustained transpirational cooling and increased leaf thermal tolerance. *Global Change Biology*, *24*(6), 2390–2402.

781 Farquhar, G. D., von Caemmerer, S., & Berry, J. A. (1980). A biochemical model of photosynthetic CO2
782 assimilation in leaves of C3 species. *Planta*, *149*, 78–90.
783 Lamour, J., Davidson, K. J., Ely, K. S., Le Moguédec, G., Leakey, A. D., Li, Q., Serbin, S. P., & Rogers, A.
784 (2022). An improved representation of the relationship between photosynthesis and stomatal
785 conductance leads to more stable estimation of conductance parameters and improves the
786 goodness-of-fit across diverse data sets. *Global Change Biology*, *28*(11), 3537–3556.
787 Leuning, R., Kelliher, F. M., de Pury, D. G. G., & Schulze, E. D. (1995). Leaf nitrogen, photosynthesis,
788 conductance and transpiration: Scaling from leaves to canopies. *Plant, Cell and Environment*, *18*,
789 1183–1200.
790 Lin, Y.-S., Medlyn, B. E., Duursma, R. A., Prentice, I. C., Wang, H., Baig, S., Eamus, D., De Dios, V. R.,
791 Mitchell, P., & Ellsworth, D. S. (2015). Optimal stomatal behaviour around the world. *Nature*
792 *Climate Change*, *5*(5), 459–464.
793 National Oceanic and Atmospheric Administration, National Aeronautics and Space Administration, &
794 United States Air Force. (1976). *US Standard Atmosphere, 1976*. US Government Printing Office.
795 https://www.ngdc.noaa.gov/stp/space-weather/online-publications/miscellaneous/us-
796 standard-atmosphere-1976/us-standard-atmosphere_st76-1562_noaa.pdf
797 Oren, R., Sperry, J. S., Katul, G. G., Pataki, D. E., Ewers, B. E., Phillips, N., & Schafer, K. V. R. (1999). Survey
798 and synthesis of intra- and interspecific variation in stomatal sensitivity to vapour pressure
799 deficit. *Plant, Cell and Environment*, *22*, 1515–1526.
800 Rodriguez-Dominguez, C. M., Buckley, T. N., Egea, G., Cires, A., Hernandez-Santana, V., Martorell, S., &
801 Diaz-Espejo, A. (2016). Most stomatal closure in woody species under moderate drought can be
802 explained by stomatal responses to leaf turgor. *Plant, Cell & Environment*, *39*(9), 2014–2026.

803 Sicangco, C. K., Sabot, M. E., Drake, J. E., Tjoelker, M. G., & Medlyn, B. E. (2026). Weighing the options: A
804 test of alternative stomatal optimisation models at high temperatures. *New Phytologist*, *250*(3),
805 1551–1568.
806